

# Forbush Decrease Data with a Simple Model

C. D'Andrea, J. Poirier, D. S. Balsara

*Department of Physics, University of Notre Dame*

*Notre Dame, Indiana, USA*

## Abstract

On October 28, 2003 an earthward-directed coronal mass ejection (CME) was observed from SOHO/LASCO imagery in conjunction with an X17 solar flare. The CME, traveling at nearly 2000 km/s, impacted the Earth on October 29, 2003 causing ground-based particle detectors to register a counting rate drop known as a Forbush decrease. In addition to affecting the rate of cosmic rays, the CME was also responsible for causing anisotropies in the direction of incidence. Data from Project GRAND, an array of proportional wire chambers, are presented during the time of this Forbush decrease. A simple model for CME propagation is proposed and we present an argument based on gyroradius that shows that a magnetic field of the radius calculated for the ejecta is sufficient to deflect energetic charged particles of an energy detectable by GRAND.

## 1 Introduction

In late October of 2003 the Earth experienced an extraordinary amount of solar and geomagnetic activity originating from solar region NOAA 10486, including an X17 flare which was one of the largest solar flares since 1976 [10]. This flare was detected beginning at 9:51 UT on October 28, 2003 (day 301) and peaked at 11:10 UT the same day. This flare had an associated CME with a transit time from the sun to the Earth of only 19 hours, making it one of the the fastest on record. The shock from the CME impacted the Earth's magnetic field as a strong sudden impulse (an abrupt increase in the horizontal component of the geomagnetic field) at 6:13 UT on October 29, 2003 (day 301) [12]. This CME caused a drop in the counting rate of ground-based cosmic ray detectors. The counting rate for neutron monitor stations remained suppressed for roughly twelve days after the impact of the shock.

Project GRAND [14], an extensive air shower array of proportional wire chambers, is a useful tool for studying the ground-level effects of cosmic rays. GRAND's median energy for vertically incident cosmic rays is 56 GeV, higher than that for neutron monitors. This allows GRAND to complement neutron monitor data by studying higher energy effects. GRAND has an angular resolution of  $0.26^\circ$  on a projected plane for incoming muon tracks. The angular

resolution, primary energy sensitivity, and large detector area of this experiment ( $82 \text{ m}^2$ ) make it an excellent instrument to study Forbush decreases. Secondary muon data obtained by GRAND during the time of the October 29 Forbush decrease are discussed. In addition, a simple model for a CME ejecta is proposed and some of the consequences of this model are discussed.

## 2 Project GRAND

Project GRAND is located at  $41.7^\circ \text{ N}$  and  $86.2^\circ \text{ W}$  at 220 meters above sea level. Its array of 64 proportional wire chamber stations are arranged in a  $8 \times 8$  grid that covers  $100 \text{ m} \times 100 \text{ m}$ . Each station contains four pairs of wire chamber planes. Each pair has a top plane with wires running north / south and a bottom plane with wires running east / west. Each plane contains 80 wire cells with a total active area of  $1.29 \text{ m}^2$ . The pairs of planes are placed vertically above one another, with a separation of 197 mm between pairs. There is a 51 mm steel plate above the bottom pair of planes, allowing muons to be differentiated from electrons (which scatter, shower, or stop in the steel). The angle of the incoming tracks is determined from the difference between the location of the wires hit on the top plane and the bottom plane. The stations have a maximum sensitivity for vertical tracks and a cutoff of  $63^\circ$  from vertical in each projected plane due to the size and separation of the planes. GRAND runs with two triggers: 1) single tracks from individual stations and 2) multiple stations in time coincidence. The data presented in this paper comes solely from trigger (1) analyzed for those single tracks which are identified as muons.

The Monte-Carlo program FLUKA [4],[5] was used to simulate primary protons in the atmosphere for energies of interest (1 - 3000 GeV). The results of these simulations were originally shown in [15] for primary protons and [16] for primary gamma rays. The results of the number of muons reaching ground level per proton of a given primary energy are shown in Figure 1. Protons were used for this simulation because the majority of the primaries which generate ground level muon counting rates are protons.

The response of GRAND to background cosmic rays can be determined by using the results from the FLUKA simulation and folding it with the cosmic ray spectrum at those angles. A primary spectrum of

$$N(E) = 1.74 \times 10^4 (E + 0.89)^{-2.75} dE \quad (1)$$

was used [7] and is shown in Figure 2. The combined response to vertical primary protons is shown in Figure 3, showing GRAND's median primary rigidity at 56 GV.

Further information on the response function and operation of Project GRAND is available from [15], [14], and references therein.

### 3 Data

The muon data rate for October 29 and 30, 2003 is shown in Figure 4. GRAND's data rate shows a decrease of 8% from the counting rate prior to the decrease. Data following the Forbush decrease show that it takes GRAND nine days to recover to its original counting rate.

In order to ensure that the data reflected only physical variations, a cut was performed to select only the best stations for analysis for this event. The r.m.s. deviation was calculated for each of the stations and compared to the expected statistical fluctuation (the square root of the mean number of counts). All stations with a ratio higher than 8.0 were eliminated from this analysis, leaving 17 stations.

Angular information for the muons was also analyzed during October 29 and October 30. The average angles in the north/south direction and the east/west direction were calculated and are shown in Figure 5. While the east/west direction shows little change in activity above statistics, the north/south angle shows a swing where more particles originate from the north during the time of the Forbush decrease. Since a Forbush decrease is caused by a large solar coronal ejection whose magnetic field deflects the incoming cosmic ray particles when it impacts the Earth, it should be expected that this causes a deficiency in particles from a particular direction.

The magnetic field near the Earth was also studied [1] during the time of this event and is shown in Figure 6. The magnetic field shows an increase during the time of the decrease which maintained for a day following the impact. This is consistent with a large coronal mass ejection with its own magnetic field interacting with the Earth's magnetic field at the time of impact. This increased magnetic field can result in a higher cutoff rigidity for cosmic rays near the Earth, resulting in a decrease in the counting rate as seen from the ground.

### 4 Theoretical Model

Decreases in cosmic-ray intensity in coincidence with changes in the magnitude of the horizontal component of the geomagnetic field (the component of the magnetic field parallel to the Earth) were first noticed by Scott Forbush in the 1930s. [11] stated that the sun would occasionally emit magnetized plasma from active regions. These clouds would affect the cosmic-ray rate in interplanetary space and produce magnetic storms on the Earth. Satellites were able to detect changes in the rate of cosmic rays (along with a simultaneous increase in magnetic field strength) in interplanetary space in 1959 and 1960 confirming this hypothesis [6]. These magnetic clouds have been identified as the ejecta from coronal mass ejections on the sun. In order to properly understand the mechanisms of Forbush decreases it is necessary to study the propagation of ejecta in the solar wind [3].

CMEs often originate in the solar corona near magnetic field lines and typically follow a coronal helmet streamer [8]. This streamer gets distorted and is

finally disrupted by the expanding closed field region underneath it. The CME speed is typically between 20 and 2000 km/s and have an average speed of 400 km/s [3] which is greater than the typical solar wind speed from the sun. When the fast ejecta meets with the slower solar wind, a shock is created [18]. It should be noted that while CMEs and flares often are associated, one is not necessary for the other.

A simple model for the propagation of the ejecta generated by a CME is presented here. With a given initial radius and magnetic field near the surface of the sun, the intended goals are to determine how it propagates through the solar system, the time of flight from the sun to the Earth, the magnetic field of the ejecta when it reaches the Earth, and the extent of the ejecta at Earth. The information on the size and magnetic field will be used to evaluate the prospect that high energy cosmic rays may be occluded by the material. The model presented here is a simple model that assumes a bulk size, shape, pressure, and magnetic field. This may not be the case if the structure created during the formation of the CME is maintained. The model, however, is adequate for determining scale values for the magnetic field and size of the ejecta when it impacts the Earth.

The first assumption is that it is the solar wind which is responsible for convecting the CME material to the Earth and therefore the flight time for the CME ejecta is connected to the solar wind. Any relative motion between the CME ejecta and the solar wind would dissipate as a shock or pressure fluctuation. The time scale for the solar wind to travel from the sun to the Earth and the time scale of a CME ejecta transit are quite similar, positing a relationship between the two which is explored further in Section 5.

In order to construct a simple model, it is necessary to know the properties of the solar wind as it propagates from the sun to the Earth. Pressure balance between the solar wind and the CME ejecta is then used to determine the properties of the CME ejecta as they flow toward the Earth. The results of a calculation of solar wind velocity and temperature with respect to distance from the sun are given in [2], shown here as Figure 7. For the purposes of discussion in this work only the damped waves will be considered (dotted lines). These values of  $v_w$  and  $T_w$  from Figure 7 are then used to determine the density of the solar wind at a given distance from the sun using a few basic principles.

We assume that the mass of the wind is constant as it expands and that its expansion is spherically symmetric:

$$\rho_w v_w d^2 = \text{constant} \quad (2)$$

where  $d$  is the distance from the sun,  $v_w$  is the velocity of the solar wind, and  $\rho_w$  is the density of the solar wind. Also it is assumed that the wind and CME follow the ideal gas law. The mass continuity equation is used to derive an equation for the density based on initial conditions:

$$\rho_w v_w d^2 = \rho_{w0} v_{w0} d_0^2 \quad (3)$$

$$\rho_w = \frac{\rho_{w0}v_{w0}}{v_w} \left(\frac{d_0}{d}\right)^2 \quad (4)$$

This equation for density is then used to determine the density of the wind at all distances given the velocity of the solar wind and the distance from the sun. [2] gives  $\rho_0$  of  $10^8$  particles/ $cm^3$  and a  $v_{w0}$  of  $3.3 \times 10^6$  cm/s at a  $d_0 = 6.96 \times 10^{11}$  cm (one solar radius).

The pressure of the solar wind will be important in determining the size of the CME as it propagates through the solar system. The total pressure of the CME is balanced by the pressure of the solar wind. As the pressure due to the solar wind decreases, the CME expands. In this case we assume that the solar wind behaves like an ideal gas. We use  $\mu$  to represent the effective mass. From the ideal gas law, the gas pressure of the solar wind is  $P_w = R\rho_w T_w / \mu$ . There is also a contribution to the pressure in the solar wind from the interplanetary magnetic field, making the total pressure due to the solar wind (in cgs units):

$$P_w = \frac{R\rho_w T_w}{\mu} + \frac{B_w^2}{8\pi} \quad (5)$$

The values for  $\rho_w$  can be found in Equation (4) and the values for  $T_w$  are those from [2]. The values for  $B_w$  assume a Parker spiral [13] which has the form of  $B_w = B_{w0}(d_0/d)^2$ . A value of 7 nT is used for  $B_{w0}$  at a distance  $d_0 = 1$  AU. This value is a mean value of the magnitude of the IMF as recorded by ACE on October 27, 2003 [1]. The initial density of the solar wind at the sun was given in [2]. Since  $\rho_w$  can be found at all distances,  $d$ , and since  $T_w$  can be read from Figure 7,  $P_w$  can be determined at all distances,  $d$ .

In order to maintain dynamical equilibrium at each radius, the pressure of the CME ejecta continually adjusts to match that of the ambient solar wind. The CME ejecta has contributions to the pressure from magnetic pressure and gas pressure. The adiabatic equation is assumed and gives the gas pressure of the CME,  $P_c$ :

$$P_c = P_{c0} \left(\frac{\rho_c}{\rho_{c0}}\right)^\gamma \quad (6)$$

The development of  $\rho_c$  is determined by the geometry of the CME and is dependent on its formation in the solar corona and the structure of the magnetic field within it. Typically the CME structure can be complex, for example the structure given in [8] is a CME with a three-part structure, the center of which is typically an erupted solar prominence. This is surrounded by a cavity which is, in turn, surrounded by a leading plasma loop. This gives a CME structure which is a magnetic field embedding a magnetic flux rope which originates at the base near the corona. If the height of the eruption is similar to the width of the loop of the magnetic field lines, the CME will have a mostly spherical structure. If the height of the prominence is larger than the radius of the magnetic field

loop then the structure of the CME will be more cylindrical in nature. Both geometries are explored below.

For a CME with spherical geometry, the continuity equation is  $\rho_c r_c^3 = \text{constant}$ . For a CME with cylindrical geometry, the continuity equation changes to  $\rho_c r_c^2 = \text{constant}$ , where  $r_c$  is the radius of the CME ejecta. We are assuming here that cylindrical CME ejecta might arise from an arcade flare-like structure. In general, the spherical and cylindrical geometries represent two structural extremes and we can also envision an intermediate case with  $\rho_c r_o^\beta = \text{constant}$  with  $2 \leq \beta \leq 3$ . For this work we used  $\gamma\beta = 4.0$ . We explore the spherical (denoted Sph.), cylindrical (denoted Cyl.), and intermediate (denoted Int.) cases below. Substituting these relationships into the pressure equation above, we get the development of the gas pressure of the CME with respect to radius.

$$\begin{aligned} P_c &= P_{c0} \left( \frac{r_{c0}}{r_c} \right)^{3\gamma} \text{ Sph.} \\ P_c &= P_{c0} \left( \frac{r_{c0}}{r_c} \right)^{\beta\gamma} \text{ Int.} \\ P_c &= P_{c0} \left( \frac{r_{c0}}{r_c} \right)^{2\gamma} \text{ Cyl.} \end{aligned} \quad (7)$$

Conservation of magnetic flux in the CME ejecta requires that

$$B_c r_c^2 = B_{c0} r_0^2. \quad (8)$$

Combining that with the magnetic pressure and substituting this into the magnetic pressure equation gives,

$$P_{Bc} = \frac{B_{c0}^2}{8\pi} \left( \frac{r_{c0}}{r_c} \right)^4 \quad (9)$$

As a result, assuming that the CME ejecta are in pressure balance with the ambient solar wind as they propagate toward Earth, we get:

$$\begin{aligned} \frac{R\rho_w T_w}{\mu} + \frac{B_w^2}{8\pi} &= P_{c0} \left( \frac{r_{c0}}{r_c} \right)^{3\gamma} + \frac{B_{c0}^2}{8\pi} \left( \frac{r_{c0}}{r_c} \right)^4 \text{ Sph.} \\ \frac{R\rho_w T_w}{\mu} + \frac{B_w^2}{8\pi} &= P_{c0} \left( \frac{r_{c0}}{r_c} \right)^{\beta\gamma} + \frac{B_{c0}^2}{8\pi} \left( \frac{r_{c0}}{r_c} \right)^4 \text{ Int.} \\ \frac{R\rho_w T_w}{\mu} + \frac{B_w^2}{8\pi} &= P_{c0} \left( \frac{r_{c0}}{r_c} \right)^{2\gamma} + \frac{B_{c0}^2}{8\pi} \left( \frac{r_{c0}}{r_c} \right)^4 \text{ Cyl.} \end{aligned} \quad (10)$$

The initial radius is based on the final reported radius for the October 28, 2003 CME [17] which was  $r_{c0} = 4.49 \times 10^{11}$  cm. The initial magnetic field of 1.0 G is a typical field at that distance from the sun and was chosen based on estimates made in [3]. The results were also determined for magnetic fields of 0.3 and 3.0 Gauss. This range of an order of magnitude in initial magnetic field gives information on initial magnetic pressure for the CME over the range of two orders of magnitude.  $P_{c0}$  was obtained by solving each of the equations shown in Equation (4) using initial conditions and  $r_c = r_{c0}$ . Finally,  $r_c$ , the size of the CME ejecta, was solved numerically for different values of solar wind pressure and temperature (effectively solving for  $r_c$  as a function of distance from the sun). Once that is done, Equation (8) can be used to solve for the magnetic field as a function of radius.

## 5 Comparison with Data

The flight time of the CME to reach one AU was calculated and is independent of the geometry. The flight time predicted by the model was 54 hours. The typical values for CME speeds range from 20 - 2000 km/s [3] which correspond to flight times from 21 hours to 86 days. The predicted flight time falls within this range. The measured time of flight was 19 hours.

The radial extent of the CME at 1 AU was determined for all three geometrical cases and for a range of magnetic fields. If an initial magnetic field of 1.0 G is used, the spherical situation gives a CME with a radius of 1.9 AU and the cylindrical CME has a radius of 0.60 AU and the intermediate geometry CME has a radius of 0.98 AU. The speed of the solar wind near the Earth as reported by ACE [1] during the event (5:00 - 19:00 UT) was used to determine the size of the CME. This gives a CME size of 0.54 AU. The progression of the radial size as a function of distance from the sun for all three geometries is shown in Figure 8. Figure 9 shows the radius as a function of distance for the cylindrical geometry for all three initial magnetic field strengths.

The magnetic field of the CME was also calculated at various points between the sun and the Earth. These are shown in Figure 10. Given an initial magnetic field of 1 G, the cylindrical case gives a mean magnetic field of 250 nT at 1 AU while the spherical case shows a mean field of 24 nT and the intermediate case gives a mean field of 90 nT. The range in magnetic field for the CME at 1 AU is between 6.9 and 160 nT for the spherical case while the cylindrical model yields a range between 110 and 310 nT and the intermediate model gives a range from 28 to 280 nT. Data from ACE show that the IMF fluctuates during this storm between 20 and 60 nT [1]. Figure 11 shows the progression of the magnetic field for the spherical model given the three different initial magnetic fields. A summary of the results for all three models and all initial magnetic fields is shown in Table 1.

The three models presented here provide a parameter range that agrees with the data for this event. Given the simplicity of this model, an exact fit was not expected. The spherical model gives a value for the magnetic field of the CME

at Earth that is consistent with that observed during the Forbush decrease of October 29, 2003 where The cylindrical model gives a value for the CME radius more consistent with the data. It is also interesting to note that the CME observed is from one of the largest flares on record and is most likely different from a “typical” CME. This model is adequate if used as a scaling argument.

If it is assumed that GRAND’s drop of 8% in its counting rate is caused by an increased magnetic field which prohibits lower energy primaries from reaching the Earth, the minimum energy primaries observed by GRAND during the decrease can be determined. Eliminating the lower 8% of GRAND’s cosmic rays leaves primaries with energies above 10 GeV. Given  $pc = Br$ , where  $pc$  is effectively the energy of a charged particle,  $B$  is the magnetic field, and  $r$  is the gyroradius for a particle in that field, a 10 GeV particle in a 24 nT field has a gyroradius of 0.0087 AU, larger than the Earth’s radius and much smaller than the size of the CME. This implies that a magnetic field of the size and strength calculated is strong enough to have an effect on GRAND’s counting rate.

## 6 Conclusions

Project GRAND sees an 8% drop in its secondary muon counting rate during the Forbush decrease of October 29, 2003. A shift is also observed in the mean angle of incident muons in the north-south plane. A simple model for the propagation of a CME through the solar system is presented. Within a range of initial conditions for the CME, the model is consistent with satellite observations near Earth during the October 29, 2003 storm.

## 7 Acknowledgments

We thank Mitch Wayne and quarknet, Michael Wiescher and JINA, and Terry Rettig for funding and support. We thank Nathan Johnson-McDaniel for his assistance. D. S. Balsara acknowledges support via NSF grants R36643-7390002, AST-005569-001, AST-0607731 and NSF-PFC grant PHY02-16783. Project GRAND was constructed through grants from the National Science Foundation and is funded through the University of Notre Dame and private donations.

## References

- [1] The ACE science website (2003) <http://www.srl.caltech.edu/ACE>
- [2] Axford W. I., J. F. McKenzie, G. V. Sukhorukova, M. Banaszkiewicz, A. Czechowski, and R. Ratkiewicz (1999), Acceleration of the High Speed Solar Wind in Coronal Holes *Space Science Reviews*, 87, 25–41.
- [3] Cane, H. V. (2000), Coronal Mass Ejections and Forbush Decreases. *Space Science Reviews*, 99, 53–77.



Figure 1: Results from primary protons simulated by the FLUKA Monte Carlo code. The R-value is the number of muons reaching ground level, on average, from a primary proton with the given energy. The dashed line represents vertically incident particles while the solid lines below the dashed represent (from top to bottom) 13°, 26°, and 39° inclination from vertical.

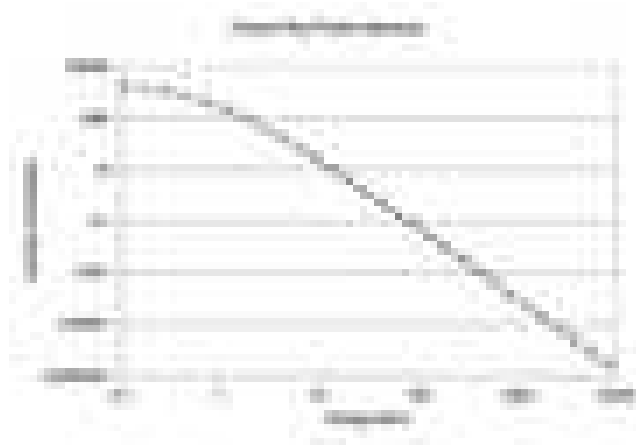


Figure 2: The graphical representation of the primary proton spectrum of  $N(E) = 1.74 \times 10^4 (E + 0.89)^{-2.75} dE$  given by [7].

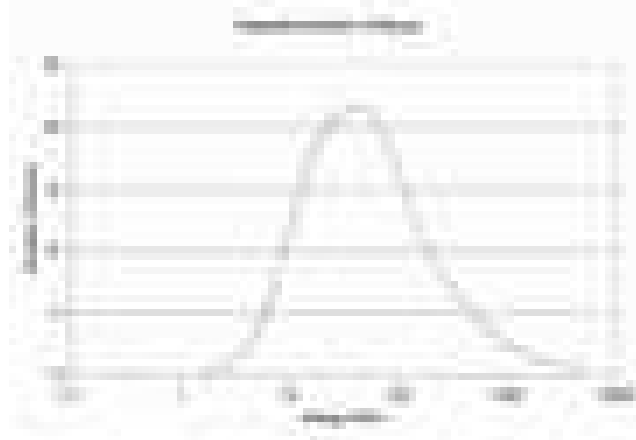


Figure 3: GRAND's sensitivity to primary protons of various energies. GRAND is most sensitive to vertical protons with an energy of 56 GeV.

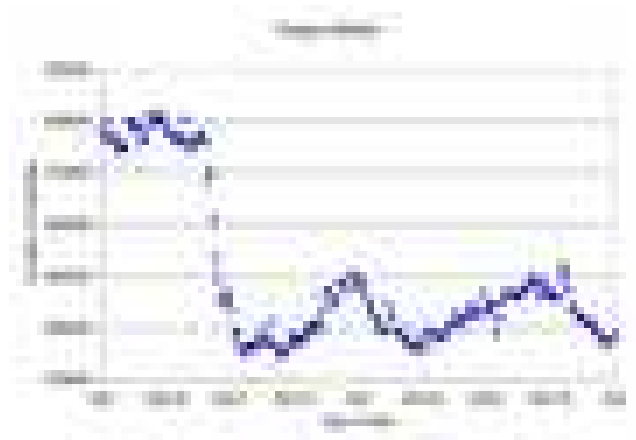


Figure 4: Data from Project GRAND and Nagoya for October 28, 2003 (D301) and the following day. The data show the counting rate for each 15 minute bin. There is an 8% decrease due to the Forbush decrease.

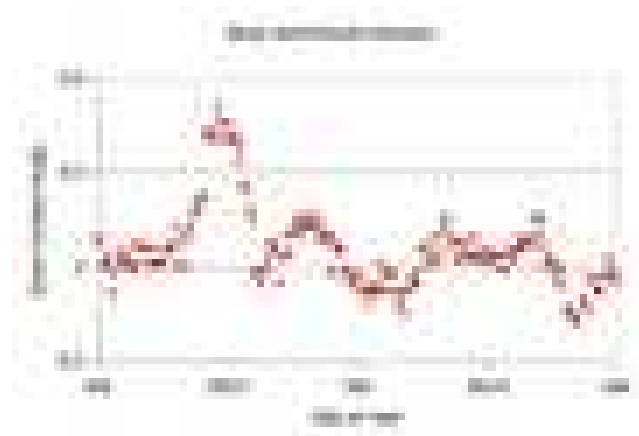


Figure 5: GRAND's angular data expressed as the mean angle (in degrees) in the north/south direction. Note the variation in the north/south direction during the time of the Forbush decrease.

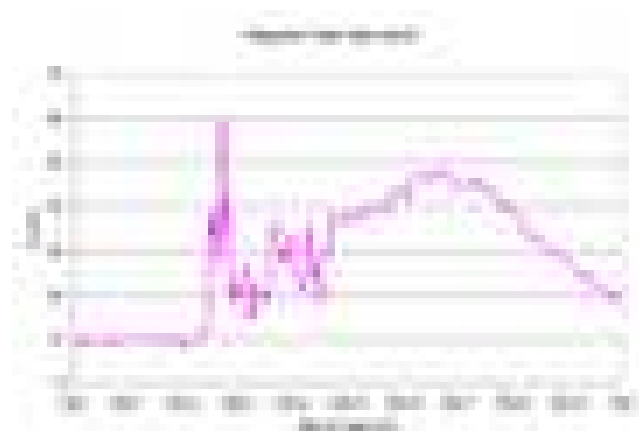


Figure 6: Magnetic field data from ACE for October 29, 2003 (Day 302). Note the quiet magnetic field ( $B \leq 10$  nT (1 nanotesla =  $10^{-5}$  Gauss)) before the arrival of the CME and the sharp increase at the time of arrival.

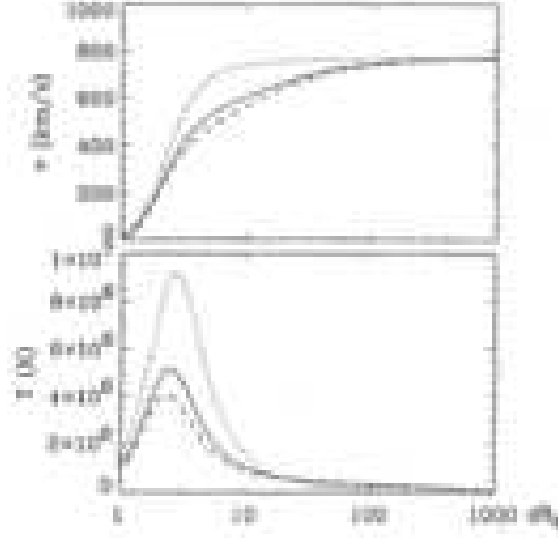


Figure 7: The solar wind velocity and temperature versus distance from the sun. This shows the effect of a fraction of undamped waves on the fast solar wind model. Dotted line (all waves damped), full line (5% undamped), dashed line (10% undamped). This figure was originally printed in [2] as Figure 4 and is used with permission. Only the dotted lines (all waves damped) were used in this work.

| Model                            | CME Radius, $r_c$ | CME B Field, $B_c$ |
|----------------------------------|-------------------|--------------------|
| $S_{0.3}$ : Sph.; $B_{c0}=0.3$ G | 1.7 AU            | 6.9 nT             |
| $S_1$ : Sph.; $B_{c0}=1$ G       | 1.9 AU            | 24 nT              |
| $S_3$ : Sph.; $B_{c0}=3$ G       | 2.0 AU            | 160 nT             |
| $I_{0.3}$ : Int.; $B_{c0}=0.3$ G | 0.98 AU           | 28 nT              |
| $I_1$ : Int.; $B_{c0}=1$ G       | 0.98 AU           | 90 nT              |
| $I_3$ : Int.; $B_{c0}=3$ G       | 0.98 AU           | 280 nT             |
| $C_{0.3}$ : Cyl.; $B_{c0}=0.3$ G | 0.50 AU           | 110 nT             |
| $C_1$ : Cyl.; $B_{c0}=1$ G       | 0.59 AU           | 250 nT             |
| $C_3$ : Cyl.; $B_{c0}=3$ G       | 0.94 AU           | 310 nT             |

Table 1: This table gives the values for CME radius and magnetic field for each of the three models with each of the three initial magnetic fields used in this paper.



Figure 8: The radius of the CME at various distances from the sun as predicted by the CME models in this paper. Circles represent the spherical model, squares represent the cylindrical model and diamonds represent the intermediate model. All the models assumed an initial CME magnetic field of 1 G (1 nanotesla =  $10^{-5}$  Gauss).

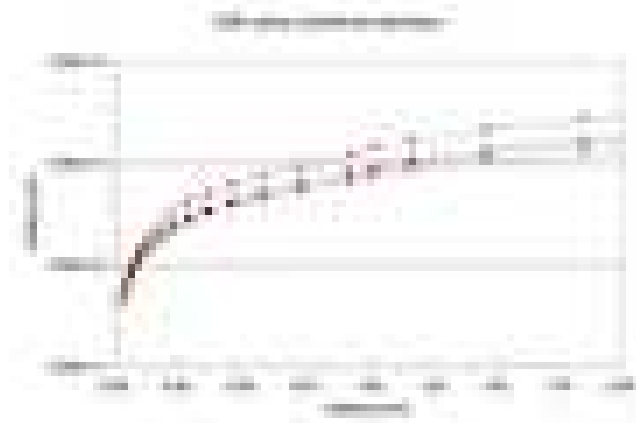


Figure 9: The progression of the radius of the CME using the cylindrical model for three different values for its initial magnetic field. Solid lines denote an initial value for the magnetic field of 1 G while the dashed lines below and above the solid lines denote initial conditions of 0.3 G and 3 G, respectively.



Figure 10: The magnetic field of the CME at various distances from the sun as predicted given by the CME models in this paper. Circles represent the spherical model, squares represent the cylindrical model and diamonds represent the intermediate model. All models in this figure used a 1 G initial magnetic field for the CME.

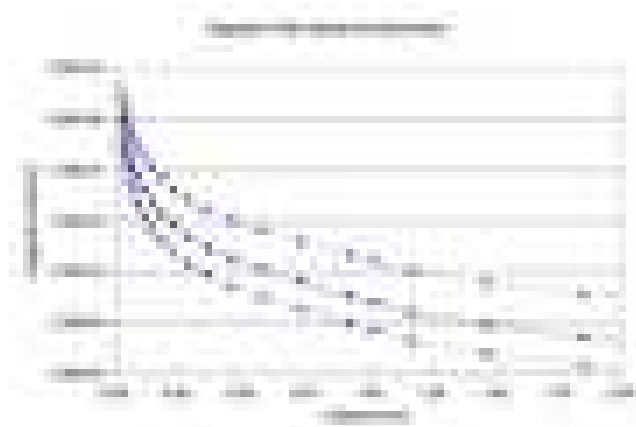


Figure 11: The progression of the magnetic field of the CME as a function of distance from the sun using the spherical model and three different initial magnetic field values. Solid lines denote an initial value for the magnetic field of 1 G while the dashed lines above and below the solid lines denote initial conditions of 0.3 G and 3 G, respectively.

- [4] Fassò, A., A. Ferrari, and P. R. Sala (2000), Electron-photon transport in FLUKA: Status, *Proceedings of the Monte Carlo 2000 Conference, Lisbon*, 159–164.
- [5] Fassò, A., A. Ferrari, P. R. Sala, and J. Ranft (2000) FLUKA: Status and Prospective for Hadronic Applications, *ibid*, 955–960.
- [6] Forbush, S. (1957), Solar Influences on Cosmic Rays, *Proceedings of the National Academy of Science*, 43, 28–41.
- [7] Fujimoto et al., "Cosmic Ray Primary Response" JCR, 76:199–141 (1978)
- [8] Gibson, S. E., B. C. Low (1998), A Time-Dependent Three Dimensional Magnetohydrodynamic Model of The Coronal Mass Ejection. *ApJ.*, 493, 460–473.
- [9] Gopalswamy, N. (2004), A Global Picture of CMEs in the Inner Heliosphere in *The Sun and the Heliosphere and Integrated System*, edited by G. Poletto and S. Suess, pp. 201–253, Kluwer Academic Press, Dordrecht, The Netherlands.
- [10] IPS 2003: <http://www.ips.gov.au/>
- [11] Morrison, P. (1956), Solar Origin of Cosmic-Ray Time Variations, *Phys. Rev.*, 101, 1397–1404.
- [12] NOAA/SEC Website (2003)  
<http://www.sec.noaa.gov/weekly/index.html>
- [13] Parker, E. N., (1958) Dynamics of the Interplanetary Gas and Magnetic Fields. *ApJ*, 128, 664–676.
- [14] Poirier, J., C. D’Andrea, M. Lopez del Puerto, E. Strahler, and J. Vermedahl (2003), A Proportional Wire Chamber Array: GRAND’s status. *Proceedings XXVII International Cosmic Ray Conference (Tsukuba)*, 993–996.
- [15] Poirier, J. and C. D’Andrea (2002), Ground level muons in coincidence with the solar flare of April 15, 2001, *J. Geophys. Research, Space Physics* Vol. 107, 1376–1384.
- [16] Poirier, J., S. Roesler, and A. Fassò (2002) Distributions of Secondary Muons at Sea Level from Cosmic Gamma Rays Below 10 TeV, *Astroparticle Phys.*, textit17, 441–458.
- [17] Solar and Heliospheric Observatory website (2003)  
<http://sohowww.nascom.nasa.gov/>
- [18] Sokolov, I. V., I. I. Roussev, T. I. Gombosi, M.A. Lee, J. Kóta, T.G. Forbes, W. B. Manchester, and J. I. Sakai (2004), A New Field Line Advection Model for Solar Particle Acceleration. *ApJ*, 616, L171–L174.